

# Bulk photovoltaic effects in altermagnets

Motohiko Ezawa<sup>1</sup>

<sup>1</sup>*Department of Applied Physics, The University of Tokyo, 7-3-1 Hongo, Tokyo 113-8656, Japan*

(Dated: December 24, 2024)

The bulk photovoltaic effect is a photocurrent generation from alternating electric field, which is a promising candidate for future efficient solar cell technology. It is the second-order optical current, which is the injection current or the shift current. We focus on the direct current generation. We show the linearly (circularly) polarized light can generate injection (shift) current in the  $d$ -wave altermagnet coupled with the Rashba interaction when the Néel vector points in an in-plane direction. The magnitude of the injection current does not depend on the frequency  $\omega$  of the applied light provided it is smaller than a certain critical frequency  $\omega_c$  and larger than the bulk gap energy  $\varepsilon_{\text{gap}}$ ,  $\varepsilon_{\text{gap}} \leq \hbar\omega \leq \hbar\omega_c$ . Hence, the use of the injection current is quite efficient for solar cell technology because any photon whose energy is within this range can be equally utilized.

**Introduction:** Nonlinear optical responses are fascinating, upon which there are intensive researches. When we apply an alternating electric field  $E(\omega)$  with the frequency  $\omega$ , there are two types of the second-order responses. One is the second-harmonic generation proportional to  $2\omega$ . The other is a direct current (dc) generation. The latter is important in the context of photovoltaic effects. Recently, bulk photovoltaic effects[1–6] including the injection current[4, 5, 7–12] and the shift current[2–5, 8–18] attract much attention because they provide more efficient photovoltaic effects than the usual one based on the  $p$ - $n$  junction for the application to solar cell devices. Indeed, only the photon having the same energy  $\hbar\omega$  as the band gap is transformed to a current in the  $p$ - $n$  junction. On the other hand, the second-order current is generated for the photon with the energy larger than the band gap, which is the injection current or the shift current. Especially, the linearly (circularly) polarized light can generate the injection (shift) current in magnetic systems. There are several experimental observation of bulk photovoltaic effects[19–23].

Altermagnets constitute one of the most active fields of condensed matter physics[24–26]. It has zero net magnetization as in the case of an ordinary antiferromagnet, but breaks time-reversal symmetry and has a momentum dependent energy spectrum[24–33]. These features open a way to future ultra-high density spintronic memories with ultrafast switching in the order of ps[34] because there is no stray field owing to the zero net magnetization. There are some studies on nonlinear responses as well on the altermagnet[35–37].

In this paper, we study photovoltaic effects in the  $d$ -wave altermagnet with the Rashba interaction, where the Néel vector points to an in-plane direction. The dc current generation by the second-order optical process is studied. We summarize the results in Fig.1. The photocurrent generation occurs only when the energy of a photon is within a certain range  $\varepsilon_{\text{gap}} \leq \hbar\omega \leq \hbar\omega_c$ , where  $\varepsilon_{\text{gap}}$  is the bulk gap energy and  $\omega_c$  is the critical frequency. A photon contributes to the shift current but the efficiency decreases for large energy as  $1/\omega$  as in Fig.1(b). On the other hand, a photon contributes equally to the injection current irrespective of  $\omega$  as in Fig.1(c). Hence, it would be useful to employ the  $d$ -wave altermagnet to generate the injection current for future solar cell technology. Incidentally, in the  $p$ - $n$  junction, only a photon whose energy is identical to the bulk gap  $\varepsilon_{\text{gap}}$  contributes to the current ( $\hbar\omega = \varepsilon_{\text{gap}}$ )

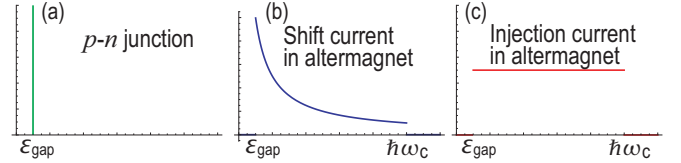


FIG. 1. Illustration of photovoltaic current as a function of the energy  $\hbar\omega$  of the photon. (a) In the case of the  $p$ - $n$  junction, only a photon with the energy  $\hbar\omega = \varepsilon_{\text{gap}}$  contributes to the current. (b) A photon with the energy  $\varepsilon_{\text{gap}} \leq \hbar\omega \leq \hbar\omega_c$  contributes to the shift current but the efficiency decreases for large energy as  $1/\omega$ , where  $\hbar\omega_c$  is a certain critical photon energy. (c) A photon with the energy  $\varepsilon_{\text{gap}} \leq \hbar\omega \leq \hbar\omega_c$  contributes equally to the injection current irrespective of  $\omega$ . The vertical axis is the magnitude of photovoltaic current, while the horizontal axis is the energy  $\hbar\omega$  of the applied photon.

as in Fig.1(a).

**Injection current and shift current:** The current density  $j$  induced by the applied electric field  $E$  is expanded as

$$j^c = \sigma^{c;a} E_a + \sigma^{c;ab} E_a E_b + \dots \quad (1)$$

The first term is the linear response and the second term is the second-order nonlinear response. If we apply an alternating electric field, the second-order response has a form

$$j^c(\omega_1 + \omega_2) = \sigma^{c;ab}(\omega_1 + \omega_2; \omega_1, \omega_2) E_a(\omega_1) E_b(\omega_2). \quad (2)$$

In this paper, we investigate the dc current generation,

$$j^c(0) = \sigma^{c;ab}(0; \omega, -\omega) E_a(\omega) E_b(-\omega). \quad (3)$$

In the following, we use the abbreviation  $j^c \equiv j^c(0)$  and  $\sigma^{c;ab}(\omega) \equiv \sigma^{c;ab}(0; \omega, -\omega)$ .

The injection current is in general given by the formula[4, 5, 7–12]

$$\begin{aligned} \sigma_{\text{inject}}^{c;ab} = & -\tau \frac{2\pi e^3}{\hbar^2} \int \frac{d^3k}{(2\pi)^3} \sum_{n,m} (f_n - f_m) \Delta_{mn}^c \\ & \times r_{nm}^b r_{mn}^a \delta(\omega_m - \omega_n - \omega), \end{aligned} \quad (4)$$

where  $\tau$  is the relaxation time,  $a$  is the lattice constant,  $f_n = 1/(\exp(\varepsilon_n - \mu) + 1)$  is the Fermi distribution function for the band  $n$ ,  $\mu$  is the chemical potential,  $\varepsilon_n$  is the energy of

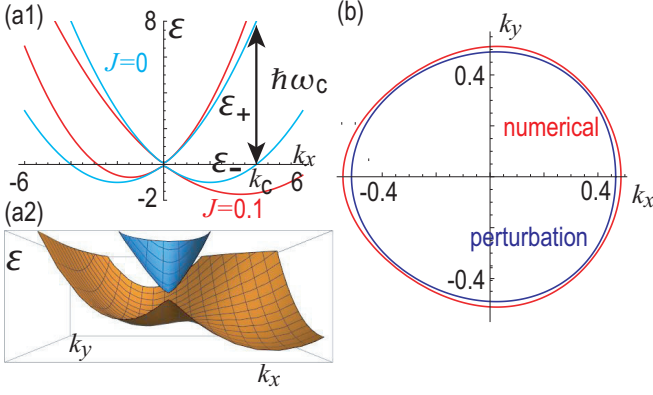


FIG. 2. (a1) Energy spectrum  $\varepsilon_{\pm}(\mathbf{k})$ . The vertical axis is the energy  $\varepsilon$  in units of  $E_0 = M\lambda^2/2\hbar^2$ . The horizontal axis is  $k_x$  in units of  $k_0 = M\lambda/2\hbar^2$ . The red and cyan curves represent the energy spectrum in the case of  $J = 0.1E_0/k_0^2$  and  $J = 0$ , respectively. (a2) Bird's eye's view in the case of  $J = 0.1E_0/k_0^2$ . (b)  $k(\phi)$  at  $\hbar\omega = 0.4E_0$  in the case of  $J = 0.1E_0/k_0^2$ . The red ellipse is the Fermi surface of the original model, while the blue ellipse is that of the perturbation theory given in Eq.(13). We have set  $B = 0.1E_0$ .

the band  $n$ ,  $r_{mn}^a = \langle m | i\partial_{k_a} | n \rangle$  is the Berry connection and  $\Delta_{mn}^c = v_{mm}^c - v_{nn}^c$  is the interband transition of the velocity  $v_{mn}^c = \frac{1}{\hbar} \langle m | \partial_{k_c} H | n \rangle$ . The injection current is nonzero when the velocity of the energy dispersion is imbalanced between the conduction and valence bands along the  $c$  direction.

On the other hand, the shift current is in general given by the formula[2–5, 8–18]

$$\sigma_{\text{shift}}^{c;ab} = -\frac{\pi e^3}{\hbar^2} \int \frac{d^3k}{(2\pi)^3} \sum_{n,m} (f_n - f_m) (R_{mn}^{c,a} - R_{nm}^{c,b}) \times r_{nm}^b r_{mn}^a \delta(\omega_m - \omega_n - \omega), \quad (5)$$

where  $R_{mn}^{c,a} = r_{mm}^c - r_{nn}^c + i\partial_{k_c} \log r_{mn}^a$  is the shift vector[5]. The shift vector is gauge invariant although the Berry connection is not gauge invariant. The shift vector describes the mean position of the Wannier function. The shift current is nonzero when the mean positions are different between the conduction and valence bands.

It is known that the injection (shift) current is generated by the linearly (circularly) polarized light in magnetic system due to the time-reversal symmetry breaking[10, 11, 38–44].

**Altermagnet:** We consider a two-dimensional system made of the  $d$ -wave altermagnets with the Rashba interaction, whose Hamiltonian is given by[24–26]

$$H(\mathbf{k}) = \frac{\hbar^2(k_x^2 + k_y^2)}{2M} I_2 + \lambda(k_x\sigma_y - k_y\sigma_x) + J(k_x^2 - k_y^2) \mathbf{n} \cdot \sigma + B\sigma_z, \quad (6)$$

where  $M$  is the effective mass of the free electrons,  $I_2$  is the  $2 \times 2$  identity matrix,  $\lambda$  is the magnitude of the Rashba interaction,  $J$  is the magnitude of the  $d$ -wave altermagnetization, and  $\mathbf{n}$  is the Néel vector of the  $d$ -wave altermagnet. We set  $\mathbf{n} = (0, 1, 0)$ . The Rashba interaction is introduced by placing

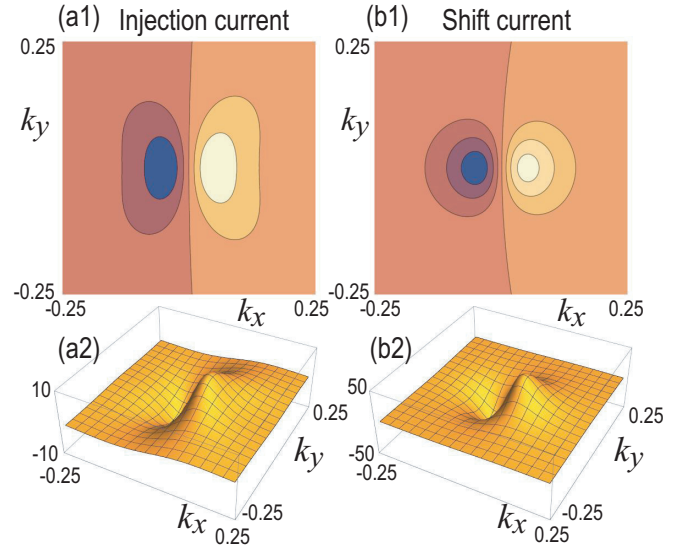


FIG. 3. (a1), (a2)  $\Delta_{+-}^x |r_{+-}^x|^2$  in the  $k_x$ - $k_y$  plane for the injection current. (b1), (b2)  $\text{Re}(R_{+-}^{x,x} - R_{-+}^{x,y}) r_{+-}^y r_{+-}^x$  in the  $k_x$ - $k_y$  plane for the shift current. (a1), (b1) Contour plot. (a2), (b2) Bird's eye's view. We have set  $J = 0.1E_0/k_0^2$  and  $B = 0.1E_0$ .

an altermagnet on the substrate[24–26, 36, 37, 45–48]. The last term  $B\sigma_z$  is introduced by magnetization, or by applying an external magnetic field, or by the Edelstein effect due to the Rashba splitting under in-plane electric field.

The  $d$ -wave magnet in two dimensions is realized in organic materials[27], perovskite materials[30], and twisted magnetic Van der Waals bilayers[49]. The  $d$ -wave altermagnet in three dimensions is realized in  $\text{RuO}_2$ [50–54],  $\text{Mn}_5\text{Si}_3$ [55] and  $\text{FeSb}_2$ [56].

The Rashba interaction breaks inversion symmetry, while the altermagnet term breaks time-reversal symmetry. Hence, the system breaks both inversion symmetry and time-reversal symmetry. The inversion symmetry breaking is necessary for the presence of the second-order optical responses. We assume  $|J| < \hbar^2/(2M)$  so that the parabolic dispersion is positive for large  $k = |\mathbf{k}|$ .

**Photovoltaic effects:** The Hamiltonian (6) is of the form,

$$H = h_0(\mathbf{k}) I_2 + \sum_{j=x,y,z} h_j(\mathbf{k}) \sigma_j, \quad (7)$$

describing a two-band system. The energy spectrum consists of  $\varepsilon_{\pm}(\mathbf{k}) = h_0(\mathbf{k}) \pm \varepsilon(\mathbf{k})$  with  $\varepsilon(\mathbf{k}) = \sqrt{\sum_{j=x,y,z} h_j^2}$ .

The energy spectrum is illustrated in Fig.2(a), where there is a Dirac cone at the  $\Gamma$  point ( $k_x = k_y = 0$ ) with the bulk band gap  $\varepsilon_{\text{gap}} = 2|B|$ . We set the chemical potential zero ( $\mu = 0$ ). We now examine the condition imposed on the frequency  $\omega$  for the photocurrent generation to occur. The optical transition occurs from the occupied valence band ( $f_- = 1$ ) to the unoccupied conduction band ( $f_+ = 0$ ) at the energy  $\varepsilon_+ - \varepsilon_- = 2\varepsilon = \hbar\omega$ . Thus, we may set  $f_- - f_+ = 1$  in the injection current (4) and the shift current (5). Furthermore, by examining the energy spectrum in Fig.2(a), the optical transition is found to occur only when the frequency  $\omega$  of a photon

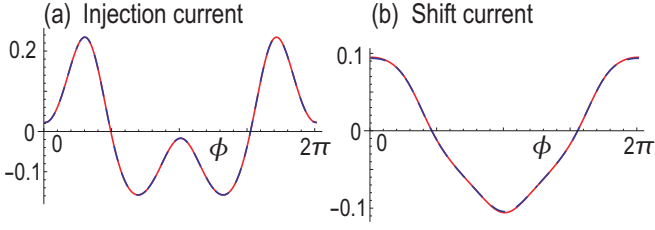


FIG. 4. (a)  $\Delta_{+-}^x |r_{+-}^x|^2$  as a function of  $\phi$  for the injection current. (b)  $\text{Re}(R_{+-}^{x,x} - R_{+-}^{x,y}) r_{-+}^y r_{+-}^x$  as a function of  $\phi$  for the shift current. The blue curves are the numerical results without using the perturbation theory, while the red curves are the analytical results based on the perturbation theory. We have set  $\hbar\omega = 0.4E_0$ ,  $J = 0.1E_0/k_0^2$  and  $B = 0.1E_0$ .

is within the range  $\varepsilon_{\text{gap}} < \hbar\omega < \hbar\omega_c$ , where the critical frequency  $\omega_c$  is determined as  $\hbar\omega_c = 2\varepsilon(k_c)$  with the use of  $k_c$  which is the solution of  $\varepsilon_-(k_c) = 0$  for the conduction band.

We study the injection (shift) current under the linearly (circularly) polarized light. We may set  $m = +$  and  $n = -$  in Eqs.(4) and Eq.(5) for a two-band system. It is straightforward to derive the formula

$$\begin{aligned} \sigma_{\text{inject}}^{x;xx} &= -\tau \frac{2\pi e^3}{\hbar^2 W} \int \frac{k dk d\phi}{(2\pi)^2} (f_- - f_+) \Delta_{+-}^x r_{-+}^x r_{+-}^x \delta\left(\frac{2\varepsilon}{\hbar} - \omega\right) \\ &= -\tau \frac{2\pi e^3}{(2\pi)^2 \hbar^2 W} \int k \frac{\Delta_{+-}^x |r_{+-}^x|^2}{2 |\partial_k E| / \hbar} \Bigg|_{k=k_\omega(\phi)} d\phi \end{aligned} \quad (8)$$

for the injection current (4), and

$$\begin{aligned} \sigma_{\text{shift}}^{x;xy} &= -\frac{\pi e^3}{\hbar^2 W} \int \frac{k dk d\phi}{(2\pi)^2} (f_- - f_+) (R_{+-}^{x,x} - R_{+-}^{x,y}) r_{-+}^y r_{+-}^x \\ &\quad \times \delta\left(\frac{2\varepsilon}{\hbar} - \omega\right) \\ &= -\frac{\pi e^3}{(2\pi)^2 \hbar^2 W} \int k \frac{(R_{+-}^{x,x} - R_{+-}^{x,y}) r_{-+}^y r_{+-}^x}{2 |\partial_k E| / \hbar} \Bigg|_{k=k_\omega(\phi)} d\phi \end{aligned} \quad (9)$$

for the shift current (5), where  $W$  is the width of the sample given by  $W^{-1} = (2\pi)^{-1} \int dk_z$ . We have introduced the polar coordinate of the momentum,  $k_x = k \cos \phi$ ,  $k_y = k \sin \phi$ , and  $k_\omega(\phi)$  is given by solving  $2\varepsilon(k_\omega(\phi)) = \hbar\omega$ .

It is notable that the injection current and the shift current do not depend on the effective mass  $M$ . This is because the Berry connection  $r_{mn}^a$ , the interband transition of the velocity  $\Delta_{mn}^c$  and the shift vector  $R_{mn}^{c,a}$  are solely determined by the  $h_j$  with  $j = x, y, z$ .

We determine the critical frequency  $\omega_c$  exactly in the case of  $J = 0$ . The condition  $\varepsilon_-(\mathbf{k}_c) = \varepsilon_-(k_c, \phi_c) = 0$  gives

$$k_c = \sqrt{2} \sqrt{M^2 \lambda^2 + M \sqrt{M^2 \lambda^4 + B^2}}. \quad (10)$$

Then, the critical energy is obtained as

$$\hbar\omega_c = 2\varepsilon(k_c) = 2\sqrt{\lambda^2 k_c^2 + B^2}. \quad (11)$$

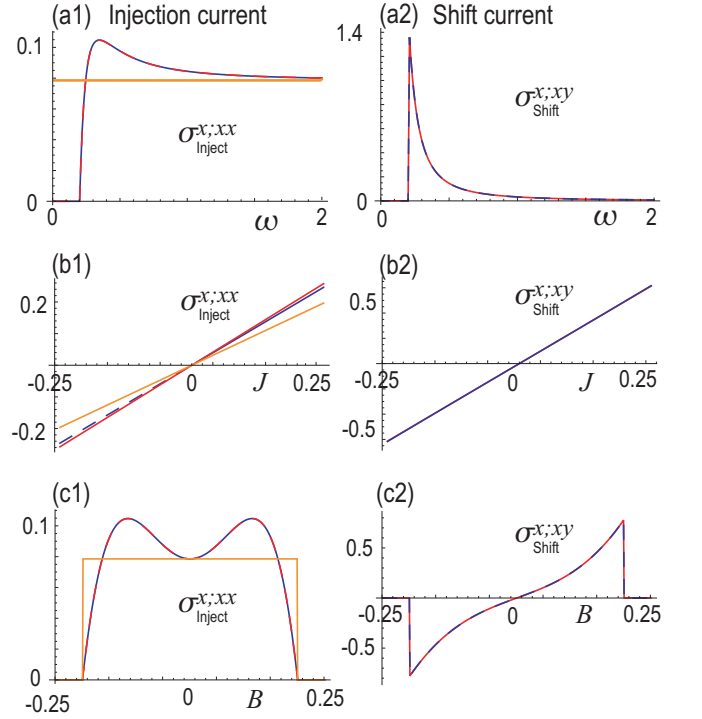


FIG. 5. (a1), (a2) Current as a function of  $\hbar\omega/E_0$ . We have set  $J = 0.1E_0/k_0^2$  and  $B = 0.1E_0$ . (b1), (b2) Current as a function of  $\frac{J}{W\lambda}$ . We have set  $B = 0.1E_0$  and  $\hbar\omega = 0.4E_0$ . (c1), (c2) Current as a function of  $B/E_0$ . We have set  $J = 0.1E_0/k_0^2$  and  $\hbar\omega = 0.4E_0$ . (a1), (b1) and (c1) Injection current  $\sigma_{\text{inject}}^{x;xx}$  in units of  $-\tau \frac{e^3}{8\hbar^2} \frac{J}{W\lambda}$ . (a2), (b2) and (c2) The shift current  $\sigma_{\text{shift}}^{x;xy}$  in units of  $\frac{e^3}{4\hbar^2} \frac{J}{W\lambda}$ . The blue curves are the numerical results without using the perturbation theory, while the red curves are the analytical results based on the perturbation theory. Orange lines are the result for  $B \ll \hbar\omega$  given in Eq.(15). The critical energy is  $\hbar\omega_c \simeq 8E_0$ .

The effect of  $J$  to  $\omega_c$  is found to be tiny comparing with the bulk band gap  $2|B|$ . We derive various formulas valid up to the first order in  $J/(W\lambda)$  in what follows.

We show the energy spectrum  $\varepsilon_{\pm}(\mathbf{k})$  along the  $k_x$  axis in Fig.2(a). It is asymmetric along the  $k_x$  direction for  $J \neq 0$ . It enables the emergence of the injection current and the shift current. The Fermi surface is shown as a red ellipse in Fig.2(b). Up to the first order in  $J/(W\lambda)$ , the energy of the Hamiltonian (6) is given by

$$\varepsilon(k, \phi) = \frac{\hbar^2 k^2}{2M} + \sqrt{\lambda^2 k^2 + B^2} + \frac{Jk^3 (\cos \phi + \cos 3\phi)}{\sqrt{\lambda^2 k^2 + B^2}}. \quad (12)$$

To calculate Eqs.(8) and (9), it is necessary to solve  $2\varepsilon(k_\omega(\phi)) = \hbar\omega$ . Solving it we obtain

$$k_\omega(\phi) = \frac{\sqrt{(\hbar\omega)^2 - 4B^2}}{2\lambda} - \frac{J \left( (\hbar\omega)^2 - 4B^2 \right) (\cos \phi + \cos 3\phi)}{8\lambda^3}. \quad (13)$$

It is shown as a cyan ellipse in Fig.2(b). It well reproduces the numerical result without using the perturbation theory shown in red ellipse.

**Injection current:** We study the injection current by applying linearly polarized light. The integrand  $\Delta_{+-}^x |r_{+-}^x|^2$  in Eq.(4) is shown in the  $k_x$ - $k_y$  plane in Fig.3(a1) and (a2). The integration is done on the ellipse  $k_\omega(\phi)$  given in Eq.(13), which is shown in Fig.4(a). The injection current Eq.(8) is obtained up to the first order in  $J/(W\lambda)$  as

$$\sigma_{\text{inject}}^{x:xx} = -\tau \frac{e^3}{8\hbar^2} \frac{J}{W\lambda} \left( 1 + 8 \left( \frac{B}{\hbar\omega} \right)^2 - 48 \left( \frac{B}{\hbar\omega} \right)^4 \right). \quad (14)$$

When the applied energy  $\omega$  is much larger than the band gap  $\varepsilon_{\text{gap}} = 2|B|$ , the injection current is independent of  $B$  and has a simple form

$$\sigma_{\text{inject}}^{x:xx} = -\tau \frac{e^3}{8\hbar^2} \frac{J}{W\lambda}, \quad (15)$$

which is the illustration in Fig.1(c). The injection current is shown as a function of  $\omega$  in Fig.5(a1), as a function of  $J$  in Fig.5(b1), and as a function of  $B$  in Fig.5(c1). The numerical result and the perturbation result well agree one to another. The injection current is almost independent of the applied frequency  $\omega$ .

**Shift current:** We study the shift current by applying circularly polarized light. The real part of  $(R_{+-}^{x,x} - R_{+-}^{x,y}) r_{+-}^y r_{+-}^x$  in Eq.(5) is shown in the  $k_x$ - $k_y$  plane in Fig.3(b1) and (b2). The integration is done on the ellipse  $k_\omega(\phi)$  given in Eq.(13), which is shown in Fig.4(b). The shift current Eq.(9) is obtained up to the first order in  $J/(W\lambda)$  as

$$\sigma_{\text{shift}}^{x:xy} = \frac{1}{\omega} \frac{e^3}{4\hbar^2} \frac{J}{W\lambda} \frac{B}{\hbar\omega} \left( 1 + 4 \left( \frac{B}{\hbar\omega} \right)^2 \right), \quad (16)$$

which is the illustration in Fig.1(b). It vanishes for the gap-

less system with  $B = 0$ . The current is generated proportional to  $1/\omega$ . The shift current is shown as a function of  $\omega$  in Fig.5(a2), as a function of  $J$  in Fig.5(b2) and as a function of  $B$  in Fig.5(c2).

**Discussion:** Bulk photovoltaic effects are useful for future solar cell technology because they produce direct current from alternating electric field. Solar light has a continuous frequency spectrum. In the view point of applications, the injection current has greater merits than the shift current. Indeed, all photons within a wide range of frequency contribute equally to the injection current. On the other hand, although the shift current is generated from all photons within the same range, the magnitude is proportional to  $1/\omega$ . Namely, the contribution from photons with high frequency  $\omega$  is small. Furthermore, the injection current has a finite contribution even for  $B = 0$ . It means that  $B$  can be infinitesimally small because it is only necessary for making a finite gap so that the Berry connection is well defined. The geomagnetism may be enough for small  $B$ . On the other hand, the shift current is proportional to  $B$ , where it is necessary to introduce large  $B$ . It is done by attaching a ferromagnet to the sample. However, it degrades the transparency to inject a light into the sample. Finally, the injection current is proportional to the relaxation time  $\tau$ . Then, the injection current is enhanced for a clean sample. On the other hand, the shift current is independent of  $\tau$ , where the shift current cannot be enhanced even for a clean sample.

The author is very much grateful to T. Morimoto and N. Nagaosa for helpful discussions on the subject. This work is supported by CREST, JST (Grants No. JPMJCR20T2) and Grants-in-Aid for Scientific Research from MEXT KAKENHI (Grant No. 23H00171).

- 
- [1] V. I. Belinicher and B. I. Sturman, The photogalvanic effect in media lacking a center of symmetry, *Sov. Phys. Usp.* 23, 199 (1980).
  - [2] W. Kraut and R. von Baltz, Anomalous bulk photo-voltaic effect in ferroelectrics: A quadratic response theory, *Phys. Rev. B* 19, 1548 (1979).
  - [3] Ralph von Baltz and Wolfgang Kraut, Theory of the bulk photovoltaic effect in pure crystals, *Phys. Rev. B* 23, 5590 (1981)
  - [4] C. Aversa and J. E. Sipe, Nonlinear Optical Susceptibilities of Semiconductors: Results with a Length-Gauge Analysis, *Phys. Rev. B* 52, 14636 (1995)
  - [5] J. E. Sipe and A. I. Shkrebtii, Second-order optical response in semiconductors, *Phys. Rev. B* 61, 5337 (2000).
  - [6] V. M. Fridkin, Bulk photovoltaic effect in noncentrosymmetric crystals, *Crystallogr. Rep.* 46, 654 (2001).
  - [7] Fernando de Juan, Adolfo G. Grushin, Takahiro Morimoto, Joel E. Moore, Quantized circular photogalvanic effect in Weyl semimetals, *Nature Communications* 8, 15995 (2017).
  - [8] F. de Juan, Y. Zhang, T. Morimoto, Y. Sun, J. E. Moore, and A.G. Grushin, Difference Frequency Generation in Topological Semimetals, *Phys. Rev. Research* 2, 012017 (2020).
  - [9] Junyeong Ahn, Guang-Yu Guo, and Naoto Nagaosa, Low-Frequency Divergence and Quantum Geometry of the Bulk Photovoltaic Effect in Topological Semimetals, *Phys. Rev. X* 10, 041041 (2020).
  - [10] Hikaru Watanabe and Youichi Yanase, Chiral Photocurrent in Parity-Violating Magnet and Enhanced Response in Topological Antiferromagnet, *Phys. Rev. X*, 11, 011001 (2021)
  - [11] Z. Dai and A. M. Rappe, Recent progress in the theory of bulk photovoltaic effect, *Chemical Physics Reviews* 4, 011303 (2023).
  - [12] J. Ahn, G.-Y. Guo, N. Nagaosa, A. Vishwanath, Riemannian geometry of resonant optical responses, *Nature Physics* 18, 290 (2022)
  - [13] S. M. Young and A. M. Rappe, First Principles Calculation of the Shift Current Photovoltaic Effect in Ferroelectrics, *Phys. Rev. Lett.* 109, 116601 (2012).
  - [14] S. M. Young, F. Zheng, and A. M. Rappe, First-Principles Calculation of the Bulk Photovoltaic Effect in Bismuth Ferrite, *Phys. Rev. Lett.* 109, 236601 (2012).
  - [15] T. Morimoto and N. Nagaosa, Topological nature of nonlinear optical effects in solids, *Science Advances* 2, e1501524 (2016)

- [16] Kun Woo Kim, Takahiro Morimoto, and Naoto Nagaosa, Shift charge and spin photocurrents in Dirac surface states of topological insulator, *Phys. Rev. B*, 95, 035134 (2017)
- [17] T. Barik and J. D. Sau, Nonequilibrium nature of nonlinear optical response: Application to the bulk photovoltaic effect, *Phys. Rev. B* 101, 045201 (2020).
- [18] Hiroki Yoshida and Shuichi Murakami, Diverging shift current responses in the gapless limit of two-dimensional systems, arXiv:2407.18565
- [19] Lukas Braun, Gregor Mussler, Andrzej Hruban, Marcin Konczykowski, Thomas Schumann, Martin Wolf, Markus Munzberg, Luca Perfetti and Tobias Kampfrath Ultrafast photocurrents at the surface of the three-dimensional topological insulator Bi<sub>2</sub>Se<sub>3</sub>, *Nature Commun.* 7, 13259 (2016)
- [20] M. Nakamura, S. Horiuchi, F. Kagawa, N. Ogawa, T. Kurumaji, Y. Tokura and M. Kawasaki, Shift current photovoltaic effect in a ferroelectric charge-transfer complex, *Nature Communications* 8, 281 (2017)
- [21] M. Sotome, M. Nakamura, J. Fujioka, M. Ogino, Y. Kaneko, T. Morimoto, Y. Zhang, M. Kawasaki, N. Nagaosa, Y. Tokura, N. Ogawa, Spectral dynamics of shift current in ferroelectric semiconductor SbSI, *PNAS* 116, 1929 (2019)
- [22] Gavin B. Osterhoudt, Laura K. Diebel, Mason J. Gray, Xu Yang, John Stanco, Xiangwei Huang, Bing Shen, Ni Ni, Philip J. W. Moll, Ying Ran and Kenneth S. Burch, Colossal mid-infrared bulk photovoltaic effect in a type-I Weyl semimetal *Nature Materials* 18, 471 (2019)
- [23] Hiroki Hatada, Masao Nakamura, Masato Sotome, Yoshio Kaneko, Naoki Ogawa, Takahiro Morimoto, Yoshinori Tokura, Masashi Kawasaki, Defect tolerant zero-bias topological photocurrent in a ferroelectric semiconductor, *PNAS* 117, 20411 (2020)
- [24] Libor Šmejkal, Jairo Sinova, and Tomas Jungwirth, Emerging Research Landscape of Altermagnetism, *Phys. Rev. X* 12, 040501 (2022).
- [25] L. Smejkal, J. Sinova, and T. Jungwirth, Beyond Conventional Ferromagnetism and Antiferromagnetism: A Phase with Non-relativistic Spin and Crystal Rotation Symmetry, *Phys. Rev. X*, 12, 031042 (2022).
- [26] L. Smejkal, A. H. MacDonald, J. Sinova, S. Nakatsuji and T. Jungwirth, Anomalous Hall antiferromagnets, *Nat. Rev. Mater.* 7, 482 (2022).
- [27] Makoto Naka, Satoru Hayami, Hiroaki Kusunose, Yuki Yanagi, Yukitoshi Motome and Hitoshi Seo, Spin current generation in organic antiferromagnets, *Nat. Com.* 10, 4305 (2019).
- [28] K.-H. Ahn, A. Hariki, K.-W. Lee, and J. Kunes, Antiferromagnetism in RuO<sub>2</sub> as d-wave Pomeranchuk instability, *Phys. Rev. B* 99, 184432 (2019).
- [29] Rafael Gonzalez-Hernandez, Libor Šmejkal, Karel Vbora, Yuta Yahagi, Jairo Sinova, Tomš Jungwirth, and Jakub Železn, Efficient electrical spin splitter based on nonrelativistic collinear antiferromagnetism, *Phys. Rev. Lett.*, 126:127701, (2021).
- [30] M Naka, Y Motome, and H Seo, Perovskite as a spin current generator. *Phys. Rev. B*, 103, 125114, (2021).
- [31] Arnab Bose, Nathaniel J. Schreiber, Rakshit Jain, Ding-Fu Shao, Hari P. Nair, Jiaxin Sun, Xiyue S. Zhang, David A. Muller, Evgeny Y. Tsybal, Darrell G. Schlom and Daniel C. Ralph, Tilted spin current generated by the collinear antiferromagnet ruthenium dioxide, *Nature Electronics* 5, 267 (2022).
- [32] Makoto Naka, Yukitoshi Motome and Hitoshi Seo, Altermagnetic Perovskites, arXiv:2411.11025
- [33] S. Hayami, Y. Yanagi, and H. Kusunose, Momentum-Dependent Spin Splitting by Collinear Antiferromagnetic Ordering, *J. Phys. Soc. Jpn.* 88, 123702 (2019).
- [34] Rina Takagi, Ryosuke Hirakida, Yuki Settai, Rikuto Oiwa, Hirotaka Takagi, Aki Kitaori, Kensei Yamauchi, Hiroki Inoue, Jun-ichi Yamaura, Daisuke Nishio-Hamane, Shinichi Itoh, Seno Aji, Hiraku Saito, Taro Nakajima, Takuya Nomoto, Ryotaro Arita and Shinichiro Seki, Spontaneous Hall effect induced by collinear antiferromagnetic order at room temperature, *Nature Materials* (2024)
- [35] Yuan Fang, Jennifer Cano, and Sayed Ali Akbar Ghorashi, Quantum Geometry Induced Nonlinear Transport in Altermagnets, *Phys. Rev. Lett.* 133, 106701 (2024).
- [36] M. Ezawa, Intrinsic nonlinear conductivity induced by quantum geometry in altermagnets and measurement of the in-plane Neel vector, *Phys. Rev. B* 110, L241405 (2024)
- [37] M. Ezawa, Third-order and fifth-order nonlinear spin-current generation in g-wave and i-wave altermagnets and perfect spin-current diode based on f-wave magnets, arXiv:2411.16036
- [38] T. Holder, D. Kaplan, and B. Yan, Consequences of Time-Reversal-Symmetry Breaking in the Light-Matter Interaction: Berry Curvature, Quantum Metric, and Diabatic Motion, *Phys. Rev. Research* 2, 033100 (2020).
- [39] Y.G. Semenov, X. Li, and K. W. Kim, Tunable Photogalvanic Effect on Topological Insulator Surfaces via Proximity Interactions, *Phys. Rev. B* 86, 201401(R) (2012).
- [40] N. Ogawa, R. Yoshimi, K. Yasuda, A. Tsukazaki, M. Kawasaki, and Y. Tokura, Zero-Bias Photocurrent in Ferromagnetic Topological Insulator, *Nat. Commun.* 7, 12246 (2016).
- [41] C.-K. Chan, N. H. Lindner, G. Refael, and P. A. Lee, Photocurrents in Weyl Semimetals, *Phys. Rev. B* 95, 041104(R) (2017).
- [42] Y. Zhang, T. Holder, H. Ishizuka, F. de Juan, N. Nagaosa, C. Felser, and B. Yan, Switchable Magnetic Bulk Photovoltaic Effect in the Two-Dimensional Magnet CrI<sub>3</sub>, *Nat. Commun.* 10, 3783 (2019).
- [43] Z. Sun, Y. Yi, T. Song, G. Clark, B. Huang, Y. Shan, S. Wu, D. Huang, C. Gao, Z. Chen et al., Giant Nonreciprocal Second-Harmonic Generation from Antiferromagnetic Bilayer CrI<sub>3</sub>, *Nature (London)* 572, 497 (2019).
- [44] Junta Iguchi, Hikaru Watanabe, Yuta Murakami, Takuya Nomoto, Ryotaro Arita, Bulk photovoltaic effect in antiferromagnet: Role of collective spin dynamics, *Phys. Rev. B* 109, 064407 (2024)
- [45] Yu-Xuan Li and Cheng-Cheng Liu, Majorana corner modes and tunable patterns in an altermagnet heterostructure, *Phys. Rev. B* 108, 205410 (2023).
- [46] Sayed Ali Akbar Ghorashi, Taylor L. Hughes, Jennifer Cano, Altermagnetic Routes to Majorana Modes in Zero Net Magnetization, *Phys. Rev. Lett.* 133, 106601 (2024).
- [47] Di Zhu, Zheng-Yang Zhuang, Zhigang Wu, and Zhongbo Yan, Topological superconductivity in two-dimensional altermagnetic metals, *Phys. Rev. B* 108, 184505 (2023)
- [48] M. Ezawa, Detecting the Neel vector of altermagnets in heterostructures with a topological insulator and a crystalline valley-edge insulator, *Physical Review B* 109 (24), 245306 (2024).
- [49] Yichen Liu, Junxi Yu, and Cheng-Cheng Liu, Twisted Magnetic Van der Waals Bilayers: An Ideal Platform for Altermagnetism, *Phys. Rev. Lett.* 133, 206702 (2024)
- [50] K.-H. Ahn, A. Hariki, K.-W. Lee, and J. Kunes, Antiferromagnetism in RuO<sub>2</sub> as d-wave Pomeranchuk instability, *Phys. Rev. B* 99, 184432 (2019).
- [51] L.Smejkal, R. Gonzalez-Hernandez, T.Jungwirth, and J. Sinova, Crystal time-reversal symmetry breaking and spontaneous Hall effect in collinear antiferromagnets. *Science Advances* 6, eaaz8809 (2020).
- [52] Teresa Tschirner, Philipp Keler, Ruben Dario Gonzalez Be-



- tancourt, Tommy Kotte, Dominik Kriegner, Bernd Buechner, Joseph Dufouleur, Martin Kamp, Vedran Jovic, Libor Smejkal, Jairo Sinova, Ralph Claessen, Tomas Jungwirth, Simon Moser, Helena Reichlova, Louis Veyrat, Saturation of the anomalous Hall effect at high magnetic fields in altermagnetic RuO<sub>2</sub>, *APL Mater.* 11, 101103 (2023)
- [53] O. Fedchenko, J. Minar, A. Akashdeep, S.W. D'Souza, D. Vasilyev, O. Tkach, L. Odenbreit, Q.L. Nguyen, D. Kutnyakhov, N. Wind, L. Wenthau, M. Scholz, K. Rossnagel, M. Hoesch, M. Aeschlimann, B. Stadtmueller, M. Klaeui, G. Schoenhense, G. Jakob, T. Jungwirth, L. Smejkal, J. Sinova, H. J. Elmers, Observation of time-reversal symmetry breaking in the band structure of altermagnetic RuO<sub>2</sub>, *Science Advances* 10, 5 (2024).
- [54] Zihan Lin, Dong Chen, Wenlong Lu, Xin Liang, Shiyu Feng, Kohei Yamagami, Jacek Osiecki, Mats Leandersson, Balasubramanian Thiagarajan, Junwei Liu, Claudia Felser, Junzhang Ma, Observation of Giant Spin Splitting and d-wave Spin Texture in Room Temperature Altermagnet RuO<sub>2</sub>, arXiv:2402.04995.
- [55] Miina Leivisk Javier Rial, Anton Badura, Rafael Lopes Seeger, Ismaa Kounta, Sebastian Beckert, Dominik Kriegner, Isabelle Joumard, Eva Schmoranzero Jairo Sinova, Olena Gomonay, Andy Thomas, Sebastian T. B. Goennenwein, Helena Reichlov Libor Smejkal, Lisa Michez, Tom Jungwirth, Vincent Baltz, Anisotropy of the anomalous Hall effect in the altermagnet candidate Mn<sub>5</sub>Si<sub>3</sub> films, *Phys. Rev. B* 109, 224430 (2024)
- [56] I. I. Mazin, K. Koepernik, M.D. Johannes, Rafael Gonzalez-Hernandez, Libor Šmejkal, Prediction of unconventional magnetism in doped FeSb<sub>2</sub>, *Proceedings of the National Academy of Sciences* 118, e2108924118 (2021)